

PCCP

Accepted Manuscript



This is an *Accepted Manuscript*, which has been through the Royal Society of Chemistry peer review process and has been accepted for publication.

Accepted Manuscripts are published online shortly after acceptance, before technical editing, formatting and proof reading. Using this free service, authors can make their results available to the community, in citable form, before we publish the edited article. We will replace this *Accepted Manuscript* with the edited and formatted *Advance Article* as soon as it is available.

You can find more information about *Accepted Manuscripts* in the [Information for Authors](#).

Please note that technical editing may introduce minor changes to the text and/or graphics, which may alter content. The journal's standard [Terms & Conditions](#) and the [Ethical guidelines](#) still apply. In no event shall the Royal Society of Chemistry be held responsible for any errors or omissions in this *Accepted Manuscript* or any consequences arising from the use of any information it contains.

ARTICLE

Effect of Anatase crystal orientation on the photoelectrochemical performance of anodic TiO₂ nanotubes

Cite this: DOI: 10.1039/x0xx00000x

Received 00th January 2012,
Accepted 00th January 2012

DOI: 10.1039/x0xx00000x

www.rsc.org/

Próspero Acevedo Peña ^{a,*}, Federico González ^a, Gonzalo González ^b and Ignacio González ^a

The TiO₂ nanotube films were prepared by anodizing Ti plates in ethylene glycol based electrolytes containing variable concentrations of ammonium fluoride and water. The morphology, optical and semiconducting properties, as well as the composition of TiO₂ films showed to be dependent on the anodizing bath composition. Among different film properties, only the preferential orientation of anatase crystals, quantified with texture coefficient of (004) plane, $TC_{(004)}$, showed the same dependence of photoelectrochemical performance on the electrolyte composition. The increased value of $TC_{(004)}$ was related to anatase crystal piling up in the [001] direction (normal to the plane of a Ti substrate), forming a fiber like texture structure along the tube that facilitates the transport of photogenerated electrons toward the conducting substrate.

Introduction

Since the work of Fujishima and Honda,¹ TiO₂ has been thoroughly studied for its application in photoelectrochemical cells due to its high stability and outstanding performance as anode.^{2–4} In order to improve the photoelectrochemical performance of TiO₂, different methodologies have been developed for its processing, having as a result films of different morphologies and properties that modulate the material's behavior.^{5–9} In recent years, obtaining TiO₂ nanotubes by anodization in electrolytes containing fluoride ions has received huge attention due to the simplicity, reproducibility and high control of morphology.^{10–12} It allows production of highly ordered structures that permit the directed electron transport towards the current collector and a high contact area with the electrolyte to carry out the oxidation reaction.

To design these structures and provide more efficient anodes, it is necessary to understand different parameters that govern the photoelectrochemical performance of TiO₂ nanotube films. Their photoelectrochemical activity has been correlated with morphological parameters,¹³ semiconducting properties,¹⁴ and anatase crystallinity.¹⁵ Recently, it has been reported the possibility of controlling the orientation of anatase crystals in TiO₂ nanotubes in the [001] direction, as a function of H₂O concentration in ethylene glycol based electrolytes, which improves the film's photoelectrochemical performance.^{16–19} This behavior has been correlated with a higher amount of anatase (001) facets exposed to the solution.^{16–18} However, although the preferred orientation was corroborated by selected area diffraction patterns, the orientation degree of anatase crystals has been measured semi-quantitatively as a function of the ratio of anatase peaks corresponding to the (004) and (200)

planes,¹⁷ thereby being difficult the detection of the real orientation degree of anatase crystals, and its relation to photoelectrochemical performance of the film. Also, even though other techniques can be used for determining crystallite orientation and distribution, such as transmission electron microscopy,^{16–18} their main drawback is a relatively small area of analysis. On the other hand, the irradiation area on the sample surface in X-ray diffraction techniques goes from hundreds of square micrometers to hundreds of square millimeters. Furthermore, the penetration depth of conventional X-ray tubes in inorganic materials is tens of times higher than that of electrons possessing conventional energies in electronic microscopes. Thus, X-ray diffraction techniques allow the analysis of textural information of samples averaged over a large area and volume at the scale of some important devices using TiO₂.

There are different approaches to the film texture determination by XRD techniques. The most accessible is by performing a conventional symmetrical reflection (CSR) measurement (as that obtained in the Bragg-Brentano geometry, in which diffraction comes only from lattice planes that are parallel to the sample surface), and then data analysis using the texture coefficient (TC). In this approach, texture characterization is achieved by comparing the observed relative peak intensity of representative Bragg reflections with those of a randomly-oriented powder standard of the same compound. However, for a strongly preferred-oriented thin film, especially that with a high morphological anisotropy, such as one having nanorods or nanotubes with a given crystallographic orientation along their longer axis, the CSR-TC approach may not be sufficient. In order to overcome this possible limitation, an alternative is to perform pole figure (PF) measurements. In this approach, the XRD is used, in particular, to determine

crystallite orientation; so that, film texture is directly obtained from the whole sample and not only from a small portion. Additionally, in films with a high morphological anisotropy, it is very useful to perform in-plane pole figure measurements. In such measurements, diffraction comes from lattice planes that are perpendicular or oblique to the sample surface, as is expected for the (101) anatase plane in a film with its crystallographic *c*-axis preferentially-oriented perpendicular to the substrate. Here, we have synthesized TiO₂ films by anodization in ethylene glycol based electrolyte with different concentrations of NH₄F and the same, unchanged concentration of H₂O, and with different concentrations of H₂O and the same, unchanged concentration of NH₄F; using the experimental strategy previously reported by the authors.^{14, 19, 20} The morphology, optical and semiconducting properties, and surface composition of the films were characterized to correlate them to their photoelectrochemical water oxidation performance. Additionally, in order to determine the texture of the TiO₂ films, we have performed measurements by two different X-ray diffraction techniques. The orientation degree of anatase crystals was quantified by texture coefficient for the (004) plane, $TC_{(004)}$, taking 10 characteristic peaks of anatase present in CSR XRD in Bragg-Brentano geometry. Alternatively, in-plane XRD figure poles for (101) and (004) planes were measured to get direct insight of preferential orientation.

1. Experimental

The TiO₂ nanotube films were obtained by potentiostatic anodization in a two electrode cell at 30 V for 2 h in ethylene glycol based electrolytes with either different NH₄F concentrations (0.05 M, 0.10 M and 0.20 M) keeping the water content constant at 1 %, or with different percentages of water (1 %, 5 %, 10 %, 25 % and 50 %) keeping the NH₄F concentration constant at 0.02 M. Pt (99.99 % Alfa Aesar) was employed as counter electrode placed at 2 cm from the Ti foil (99.95 % Alfa Aesar). The electrolyte was stirred with a magnetic bar during anodization. Finally, the films were thoroughly cleaned with ethanol and Millipore water (18.2 MΩcm), left to air dry, and heat treated in ambient air at 450 °C (10 °Cmin⁻¹) for 30 min to obtain anatase polymorph.¹⁴

SEM images were acquired using a JSM 7600F high field emission microscope, with an accelerating voltage of 10.0 kV. Morphological characteristics of the formed films were estimated using the iTEM software from Olympus soft imaging solutions. The UV-Vis diffuse reflectance spectra were measured using a Varian Cary 100 spectrometer equipped with an integration sphere. XPS analyses were performed using Thermo Scientific K-Alpha X-ray photoelectron spectrometer with a monochromatized Al Kα X-ray source (1487 eV). Since oxygen is the predominant element in this type of materials, the position of the O_{1s} peak at 531.0 eV was monitored on each sample to ensure that no binding energy shift due to charging had occurred. Narrow scans were collected at 60 eV analyzer pass energy and a 400 μm spot size. Additionally, the values obtained using the O_{1s} peak for charge compensation are closer to the TiO₂ reported values, 458.0 eV ± 0.4 eV,²¹⁻²⁶ than those obtained when C_{1s} peak is used for charge compensation.

The X-ray diffractograms of the films were measured in air at room temperature using a Bruker D8 Advance diffractometer with the Bragg Brentano θ - θ geometry, Cu-K α radiation, a Ni 0.5% Cu-K β filter in the secondary beam, and a one dimensional position sensitive silicon strip detector (Bruker, Lynxeye).^{27, 28} The diffraction intensity as a function of 2θ

angle was measured between 20° and 70°, with a 2θ step of 0.020371°, for 38 s per point. Crystalline structures were refined by the Rietveld method using a fundamental parameters approach,²⁹ as implemented in the TOPAS code, version 4.2.27. The Cu-K α X ray emission profile was modeled with the one reported by G. Hölzer et al.³⁰ The parameters used during refinements included polynomial terms for modeling of the background, and the lattice parameters; preferred orientation and the width of a Lorentzian profile for modeling the average crystallite size. Last two features were modeled in reciprocal space with a symmetrized harmonics expansion.³¹ The images of the shape of the average crystallite were generated using Medit software, release 2.3b,³² following the methodology reported by Bokhimi et al.³³ The texture analysis was measured with a Rigaku Ultima IV X-ray diffractometer with a Cu-K α radiation operating at 40 KV and 40 mA. The device has a CBO system (Cross Beam Optics) that determines a divergence angle of output beam approximately at 0.03° 0.05°. In-plane pole figures were recorded for poles (101), and (004) for three samples; the main advantage of such method in comparison with the conventional Schulz reflection method, is the possibility to record practically the whole pole figure (i.e. from $\alpha = 0^\circ$ to $\beta = 90^\circ$). For α and β scans, sampling steps of 0.4° and 1.5° were adopted, with a speed of 90° min⁻¹.

The (photo)electrochemical tests were carried out in a conventional three electrode cell equipped with a quartz window allowing the UV light illumination of the entire portion (1.23 cm²) of the TiO₂ nanotube film exposed to the electrolyte. An Ag/AgCl (3.0 M KCl) electrode was employed as reference electrode and a graphite bar (99.999 % Alfa Aesar) as counter electrode. The 0.1 M HClO₄ aqueous electrolyte used for film characterization was prepared employing Millipore water (18.2 MΩcm) and HClO₄ (JT Baker, 69 %). Before each test, the electrolyte was bubbled with N₂ gas for 30 min and N₂ atmosphere was preserved during the experiments. The illumination was made using a Newport Q Housing (Model 60025) equipped with a 100 W Hg arc lamp.¹⁴

The semiconducting properties of the films were estimated from Mott-Schottky plots. The space charge capacitance of the film was extracted from the high frequency time constant of the potentiostatic EIS spectra obtained at 50 mV intervals between 0.75 V vs. Ag/AgCl and 0.0 V vs. Ag/AgCl.¹⁴ Prior to each measurement, the measuring potential was imposed for 10 minutes in order to stabilize the interfaces, then the EIS spectra were collected in a frequency interval between 10 kHz and 10 mHz with AC perturbation of ±10 mV (peak to peak). Finally, the experimental EIS spectra were fitted to an equivalent circuit, $R(Q(R(QR)))$, using Boukamp software. The (photo)electrochemical characterization was carried out using a BAS Epsilon potentiostat and EIS measurements were performed in an EG&G PAR model 283 potentiostat/galvanostat, coupled to a SI model 1260 Solartron frequency response analyzer.

2. Results and discussion

2.1 TiO₂ nanotube film characterization

The morphology of the film obtained after 2 h of anodization at 30 V, without heat treatment, was characterized by SEM images. Top and cross sectional views of the films formed in different electrolytes are shown in Figure 1. Variation in morphology of the films is in agreement with the variation in electrolyte aggressiveness, as has been reported in previous

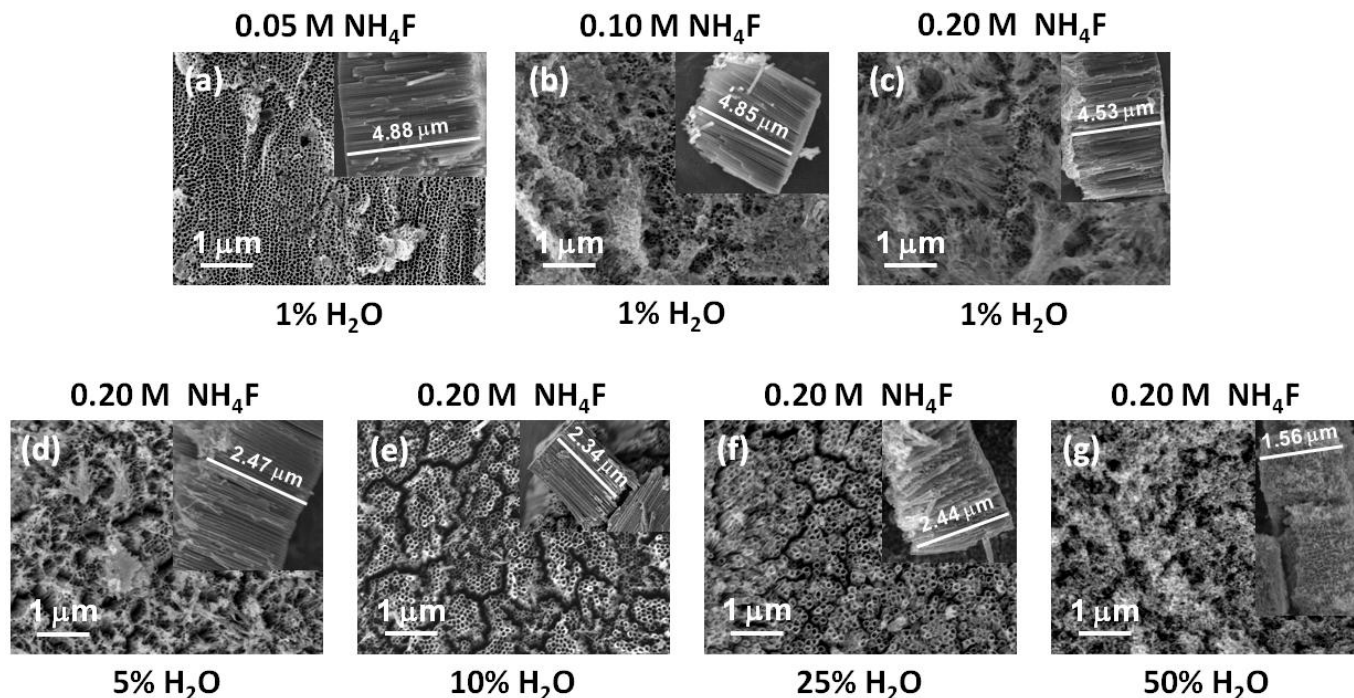


Figure 1. Effects of NH_4F concentration and H_2O percentage (indicated in figure) on the morphology of TiO_2 film obtained by anodization at 30 V for 2 h, without heat treatment.

researches.^{20, 34, 35} The ordered TiO_2 nanotube films were obtained in all cases except for the electrolyte containing 0.20 M NH_4F and 50 % H_2O (Figure 1 g), which exhibited a sponge like morphology due to considerably increased chemical attack suffered by nanotubes during anodization.

From SEM images similar to those shown in Figure 1, different morphological parameters of TiO_2 films were estimated (Table 1): internal tube diameter (d_i), tube length (l), wall thickness (w), tube to tube distance (d_t), film porosity, P , estimated from equation (1),³⁶ and the roughness factor, R , estimated from equation (2).³⁷

$$P = 1 - \frac{2\pi w(w + d_i)}{\sqrt{3}(d_i + 2w)^2} \quad (1)$$

$$R = 1 + \frac{4\pi l(w + d_i)}{\sqrt{3}(d_i + 2w)^2} \quad (2)$$

The increase in NH_4F concentration did not cause considerable variations in d_i and l , and had slight influence on film porosity. In contrast, the increase in H_2O content in the electrolyte provoked a considerable increase in d_i and a decrease in both l and w , due to a higher chemical attack of the formed oxide resulting in the greater porosity of the formed film. The value of d_i increased with NH_4F concentration and H_2O content due to the dissolution of titanium oxifluoride film formed on the tube walls during its growth.^{10-12, 20} R that represents the physical surface area of the film per unit of projected area, decreased as NH_4F concentration and H_2O content in the electrolyte increased. Voltammetric characterization (supplementary material, Figure S1) of the films heat treated at 450 °C for 30 min in the dark (10 °Cmin⁻¹) confirms an increase in the roughness factor of the films with the H_2O amount present in the anodizing bath, as well as in anodic currents measured during reverse scan.³⁸ However, the variation in NH_4F concentration did not show considerable variations in the recorded currents, which is in agreement with the variation in R observed in Table 1. The correlation between

R and voltammetric behavior of the film obtained in the dark, indicates a variation in the electroactive area of the electrodes, particularly associated with the H_2O content in the anodizing bath during film synthesis.

The films obtained and heat treated at 450 °C for 30 min (10 °Cmin⁻¹), were characterized by XPS (supplementary material, Figure S2). The spectra show no variations in Ti (Ti_{2p}) and O (O_{1s}) species, but do show them in the presence of N and F species in porous TiO_2 films, particularly that obtained at higher NH_4F concentration and lower H_2O content. The presence of these species, mainly N,³⁹ modified the optical properties of the obtained films causing a variation in the band gap (E_g) measured from the reflectance spectra using the Kubelka Munk approximation for the indirect allowed transitions (supplementary material, Figure S3). On the other hand, semiconducting properties of the films estimated by Mott-Schottky curves, also showed to be dependent on the anodizing bath composition (supplementary material, Figure S4). While a higher NH_4F concentration in the anodizing bath increases the number of N_d carriers in the film and considerably displaces E_{fb} towards less positive values, a higher H_2O content in the anodizing bath decreases N_d of the film maintaining its E_{fb} constant until a slight increase at 25 % water content, a behavior similar to that previously reported by other researchers.¹⁵

Figure 2 shows XRD patterns for all the prepared films after being heat treated at 450 °C for 30 min (10 °Cmin⁻¹). The only crystalline phase present in the films is anatase, but because of the thickness of these films, the X-ray beam penetrates until the substrate and titanium maximums also appear in diffractograms. Normally, the most intense peak for anatase is the one corresponding to (101) plane, present at ~25.3°. However, at low NH_4F concentrations (Figures 2 i and ii), the peak corresponding to (004) plane, present at ~38°, is much more intense than that of (101) plane, which indicates that depending on the conditions for the growth of TiO_2 nanotubes,

Table 1. Morphological parameters of the formed films estimated from SEM images. Internal diameter, d_i ; tube length, l ; wall thickness, w ; tube to tube distance, d_t ; porosity, P ; roughness factor, R .

[NH ₄ F] (M)	%H ₂ O	d_i^* (nm)	l^* (nm)	w^* (nm)	d_t (nm)	P	R
0.05	1	58 ± 6	4878 ± 18	10.3 ± 2.1	71 ± 7	0.72	391.9
0.10	1	59 ± 9	4853 ± 47	10.4 ± 1.3	85 ± 11	0.71	383.4
0.20	1	58 ± 10	4536 ± 50	12.0 ± 1.8	84 ± 9	0.70	343.6
0.20	5	64 ± 7	2473 ± 49	11.5 ± 2.2	92 ± 12	0.71	180.6
0.20	10	77 ± 9	2343 ± 52	9.4 ± 1.2	100 ± 11	0.75	161.2
0.20	25	94 ± 11	2443 ± 56	9.6 ± 1.9	128 ± 16	0.77	144.1
0.20	50	--	1563 ± 34	--	--	--	--

*The values reported in the table are an average of 500 measurements for d_i and w and 100 measurements for l .

they may be preferentially oriented along certain crystallographic orientation, *i.e.*, they may exhibit texture. Although this behavior has been already reported in previous works,¹⁶⁻¹⁹ there is little knowledge of its origin and its impact on the performance and properties of the film.

In order to establish the effect of film growth conditions on the crystalline properties of nanotubes, our first approximation was to extract intensities of 10 Bragg reflections appearing in the interval of 20° to 70° at 2θ, corresponding to anatase (Figure 2).

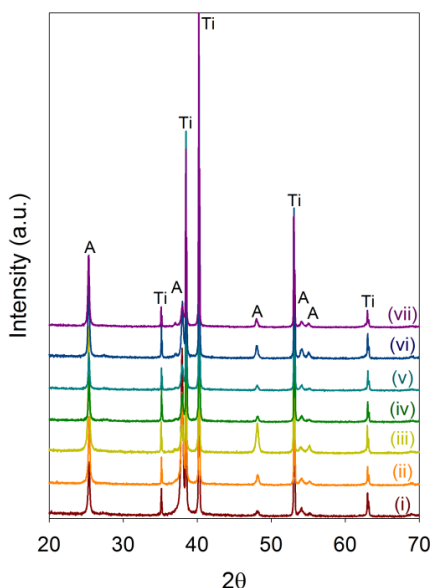


Figure 2. XRD patterns of TiO₂ films formed by potentiostatic anodization at 30 V for 2 h, in different electrolytes studied: (i) 0.05 M NH₄F, (ii) 0.10 M NH₄F, (iii) 0.20 M NH₄F in ethylene glycol with 1% H₂O, and 0.20 M NH₄F in ethylene glycol with (iv) 5% H₂O, (v) 10% H₂O, (vi) 25% H₂O and (vii) 50% H₂O.

These data were obtained from Rietveld refinement of diffractograms, including the peaks attributed to Ti. The unitcell of anatase was modelled with tetragonal symmetry described by the space group I_{41}/amd , and a basis containing one Ti⁴⁺ at the relative coordinates (0, 0, 0) and one O²⁻ at the relative coordinates (0, 0, z) with an initial z value of 0.2. The hexagonal unit cell of metallic titanium (phase α) was modelled with the symmetry described by the space group P_{63}/mmc and a basis containing only one Ti atom at the relative coordinates (1/3, 2/3, 1/4). To show the good fit between the experimental and calculated X-ray diffractograms, a typical Rietveld refinement plot is depicted in Figure S5

(supplementary material) obtained for the film grown at 30 V for 2 h in electrolyte containing 0.05 M NH₄F in ethylene glycol with 1 % H₂O and heat treated.

An intensity ratio (I_{004}/I_{101}) of about 0.20 was determined from XRD measurements of a randomly oriented and isotropic in shape commercial TiO₂ powder sample (Degussa P25), whereas the same ratio calculated from the intensities extracted from Rietveld refinements of XRD spectra of different TiO₂ films, showed values ranging from 3.79 to 0.32 (see Table 2). As the I_{004}/I_{101} ratio in the TiO₂ porous films is 1.5 to 19 times bigger than for isotropic and randomly oriented powder, it is reasonable to assume that anatase crystals are preferentially oriented with their (001) planes parallel to the Ti-substrates as a function of the anodizing bath composition. Following the approach reported by Ariosa et al.,⁴⁰ a semi quantitative estimation of the texture can be calculated using the extracted intensities from the texture coefficient (TC), defined by, equation 3.⁴¹

$$TC_{(xyz)} = \frac{I_{xyz}/I_{xyz}^0}{\frac{1}{N} \sum I_{hkl}/I_{hkl}^0} \quad (3)$$

where I_{hkl} represents the relative intensity for the (hkl) reflection, I_{hkl}^0 is the relative intensity for the (hkl) reflection for isotropic randomly oriented powder and N is the number of Bragg reflections considered (10 in our case). By definition, TC ranges from 1 (no texture) to N (single oriented crystals).⁴⁰

The texture coefficient for (004) plane, $TC_{(004)}$, and the ratio I_{004}/I_{101} for films grown at different conditions are shown in Table 2. From data in Table 2 two facts are noteworthy: 1) $TC_{(004)}$ as well as the I_{004}/I_{101} ratio decrease as NH₄F concentration increases in the anodizing bath containing 1 % H₂O, and 2) films grown at 0.20 M NH₄F with the intermediate 10 % H₂O value reach the maximum $TC_{(004)}$ (Table 2).

Table 2. Texture coefficient values for the (004) plane, $TC_{(004)}$, and I_{004}/I_{101} ratio for TiO₂ porous films grown in different anodizing baths.

[NH ₄ F] (M)	%H ₂ O	$TC_{(004)}^*$	I_{004}/I_{101}
0.05	1	6.94	3.79
0.10	1	5.57	1.69
0.20	1	2.19	0.32
0.20	5	3.81	0.84
0.20	10	4.17	1.00
0.20	25	4.03	0.80
0.20	50	2.66	0.50

* $TC_{(004)}$ estimated for anatase crystals randomly c -oriented in TiO₂ nanotubes is 2.41

Further analysis (see supplementary information for details) of the XRD data can be achieved by assuming that anatase crystals in TiO₂ nanotubes are preferentially assembled along the [001] direction of the tetragonal cell, *i.e.* they are *c*-axis oriented like nanotubes, though not fully oriented perpendicular to the substrate. According to Eq. (S1), the intensity correction factor for the (004) peak is 1, while for the intensity of the (101), which appears when the *c*-axis oriented nanotubes are tilted by $\psi_{101} = 68.3^\circ$, the intensity correction factor is 0.137. From ten calculated shape correction factors (one for each reflection) shown in Table S1, it is possible to calculate a corresponding $TC_{(004)}$ for anatase crystals randomly *c*-oriented in TiO₂ nanotubes around 2.41.

For the sample grown with 0.2 M NH₄F/1 % H₂O and 0.2 M NH₄F/50 % H₂O and considering the presence of nanotubes, it can be stated that anatase crystals are randomly oriented, since the $TC_{(004)}$ values of 2.19 and 2.66, respectively (see Table 2), are very close to the value of $TC_{(004)}$ estimated for anatase crystals randomly *c*-oriented in TiO₂ nanotubes. In the other films, there is an additional contribution besides of the purely attributable to the anisotropy (nanotube morphology) of the films. This texture is due to the *c*-axis oriented piling of the anatase crystals in the nanotubes and to the preferential orientation of these along the perpendicular direction of the Ti substrate.

Generally speaking, pole figure measurement is an XRD technique where the diffraction angle (2θ) is fixed and the diffracted intensity is collected by varying two geometrical parameters: the α angle (tilt angle from sample surface normal direction) and the β angle (φ rotation angle around sample surface normal direction). The obtained diffracted intensity data is plotted as a function of α and β . Further experimental evidence of the *c*-axis oriented piling is provided in Figure 3 through pole diagrams obtained for three different films: a) 0.05 M NH₄F/1 % H₂O, b) 0.2 M NH₄F/1 % H₂O, and c) 0.2 M NH₄F/50 % H₂O. Figure 3 shows equal area projection plots of anatase for (101) and (004) poles. A fiber like texture along [001] is observed for all the films, associated with the nanotube morphology of the films. That means circular symmetry around some sample axis (Figure 3), evidenced by a characteristic ring at $\alpha = 68.3^\circ$ (the angle between (101) and (004) planes). However, it is worth mentioning that for the sample grown in 0.05 M NH₄F/1 % H₂O, the formation of just one ring was detected (Figure 3 a), unlike the other two films (Figure 3 b and c), where diffraction intensities are distributed around the ring, as shown by the changes of intensity (color online). Consistently with the above, for (004) pole projections (Figs. 3 d, e and f), only the central spot should appear, as it is the case; however, also the reflection from (002) of Ti substrate overlaps and is strongly present with two spots, compatible with a {012} <12-1> preferred orientation ($\alpha = 42.5^\circ$) of α Ti.

Additionally to the previous texture analysis, and because the size broadening effect on the XRD peaks was treated by spherical harmonic functions, it is possible to model the shape of the crystallites. The explicit formula for the spherical harmonics treatment of size broadening is expressed by the following equation:

$$\beta_{hkl} = \frac{\lambda}{D_{hkl} \cos \theta} = \frac{\lambda}{\cos \theta} = \sum_{lmp} a_{lmp} Y_{lmp}(\Theta_{hkl}, \Phi_{hkl}) \quad (4)$$

where β_{hkl} is the size contribution to the integral breadth of reflection (hkl), $Y_{lmp}(\Theta_{hkl}, \Phi_{hkl})$ are spherical harmonic functions, and D_{hkl} is the Lorentzian crystallite size perpendicular to planes with hkl indices. Spherical harmonics (SH) up to sixth order were used. For the anatase space group

(I_{41}/amd) the physical meaning SH are Y_{00} , Y_{20} , Y_{40} , Y_{44+} , Y_{60} and Y_{64+} .

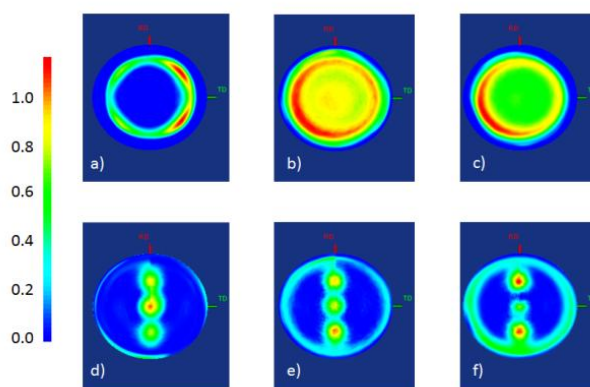


Figure 3. Plots of equal area projections of anatase, (101) and (004) poles, characterized by a ring at $\alpha = 68.3^\circ$ and a central spot, respectively. These projections are compatible with a fiber texture along [001]. Sample 0.05 M NH₄F (1 % H₂O) plots a) and d), sample 0.2 M NH₄F (1 % H₂O) plots b) and e), sample 0.2 M NH₄F (50 % H₂O) plots c) and f).

After refinements it is possible to estimate the apparent shape along each crystal direction. Figure 4 shows the average shape of the crystallite derived from the XRD line broadening for the films grown in 0.05 M and 0.2 M NH₄F (1 % H₂O). As can be seen, the disc shape of anatase crystallites in the film grown in 0.05 M NH₄F (Figure 4 a) that gives rise to a greater texture of the nanotubes, allows the piling of many crystallites in the direction perpendicular to Ti plate, as shown by pole diagram in Figure 3 a. However, the shape of crystallites of film grown in 0.2 M NH₄F (Figure 4 b), which exhibits less texture, is spherical. This is reasonable, because although anatase crystals are piled up in the direction perpendicular to Ti plate, no specific shape is necessary to allow the anisotropic piling. This proposal agrees with the findings reported by Lee et al.¹⁷ using TEM characterization of TiO₂ nanotube films with oriented and randomly oriented anatase crystals. The Selected Area Diffraction patterns of nanotube cross section with oriented anatase crystals showed that the anatase crystals are piled up in the [001] direction, parallel to the *c*-axis of nanotubes.

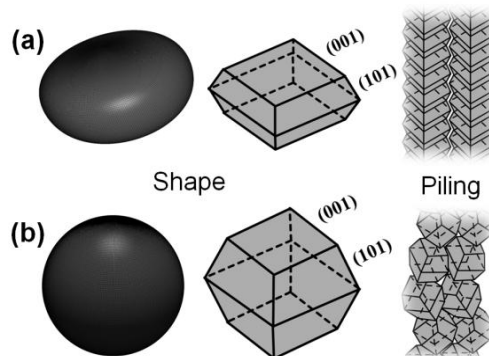


Figure 4. Shape of the average anatase crystallite in the sample (a) 0.05 M NH₄F (1 % H₂O) and (b) 0.2 M NH₄F (1 % H₂O) derived from XRD in Figure 2, treated by spherical harmonic functions. Also shown here are the schemes of the crystals and the piling based on the pole diagrams in Figure 3.

2.2 Photoelectrochemical water oxidation performance

The effect of NH_4F concentration and H_2O content in the electrolyte used for the growth of TiO_2 films on their photoelectrochemical water oxidation performance was evaluated by measuring the photocurrent generated using linear voltammetry curves (Figure 5 a and b), and potentiostatic current transients (Figure 5 c and d).

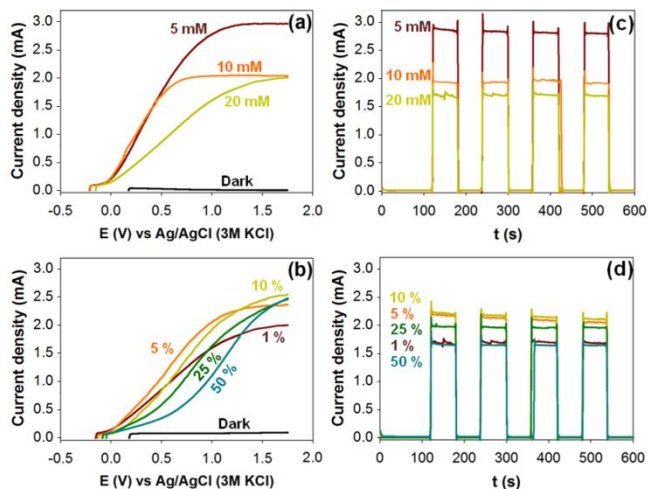


Figure 5. Photoelectrochemical water oxidation performance (0.1 M HClO_4), measured by: (a and b) linear voltammetry ($v = 20 \text{ mVs}^{-1}$), and (c and d) chronoamperometry (1.25 V vs. Ag/AgCl), for TiO_2 nanotube films previously grown at 30 V for 2 h in different electrolytes: (a) $x \text{ mM}$ NH_4F in ethylene glycol (1 % H_2O), and (b) 0.20 M NH_4F in ethylene glycol (x % H_2O), and heat treated at 450 °C.

The I vs. E curves obtained in 0.1 M HClO_4 electrolyte in the absence (dark) and presence of illumination are shown in Figure 5 (a and b), for the films prepared in ethylene glycol based electrolytes with different NH_4F concentrations (Figure 5 (a)) and different H_2O contents (Figure 5 (b)). The currents measured in the dark are much lower than those measured in the presence of illumination, showing the considerable effect of illumination on water oxidation process in TiO_2 porous films.

Additionally, potentiostatic current transients were measured by imposing an anodic potential of 1.25 V vs. Ag/AgCl, and intermittently illuminating the electrode. The measured I vs. t curves are shown in Figures 5 (c and d). After imposing the potential of 1.25 V vs. Ag/AgCl in the dark, a current rapidly decreasing over time was recorded. Upon illuminating the electrode, the current immediately increased and remained practically constant until the illumination was interrupted and got close to zero, as initially measured in the dark.

Although the disappearance of nanograss and formation of well defined nanotubular structures (Figure 1) were well correlated with the increase in photogenerated currents;⁴² however, there is no quantitative form to measure the order of the TiO_2 nanotubes and the SEM images might be subjective since there is only a small portion of the sample that is being observed. On the other hand, structural and compositional changes that influenced the observed response were also seen. For instance, the insertion of species from the electrolyte used for film anodization modified the optical and semiconducting properties of the films, particularly of that formed in the electrolyte containing 0.20 M NH_4F in ethylene glycol (1 %

H_2O). Previous studies have reported that N doping of TiO_2 leads to a decrease in E_g increasing its performance under visible light. However, this modification leads to a decreased performance of the material when it is illuminated with UV light, because oxygen vacancies created by N insertion in the material induce energy states below the conduction band which modify the electron transport through the films.³⁹ Despite all this, none of these properties can be directly related to the variation in photoelectrochemical performance of TiO_2 films prepared in this study.

Different researches have reported that the composition of electrolyte employed for the growth of TiO_2 nanotubes seems to modify anatase crystallinity in nanotubes,¹³ as well as its preferential orientation in the (001) direction,¹⁶⁻¹⁹ having direct repercussions on its photoelectrochemical performance. On comparing the dependence between the measured photocurrent from chronoamperograms in Figures 5 and $TC_{(004)}$ reported in Table 2, these two variables are seen to exhibit the same dependence on electrolyte composition, Figure 6. It is worth mentioning that even when the data in Figure 6 appears to follow only one tendency, these data comprise a wide change in the tube length and pore diameter, and comparison must be done with restraint. For example, in the left part of the Figure 6 are plotted the data for films obtained in the anodic bath with lowest water content (1 %) and different NH_4F concentration. These films showed similar length, porosity and roughness factor (see Table 1), but the preferential orientation of anatase crystals in the [001] direction seems to control the magnitude of the photocurrent measured and; furthermore, depolarize the water oxidation reaction, as observed in Figure 5 a, in which the photocurrent density rise at lower potentials for films with higher $TC_{(004)}$. On the other hand, the right part of the Figure 6 compare the photocurrent of films with different morphological properties, see Table 1, so the changes in the photocurrent can not merely be assumed to alteration in the $TC_{(004)}$, even when undoubtedly this factor contributes to the photoelectrochemical behaviour of the film.

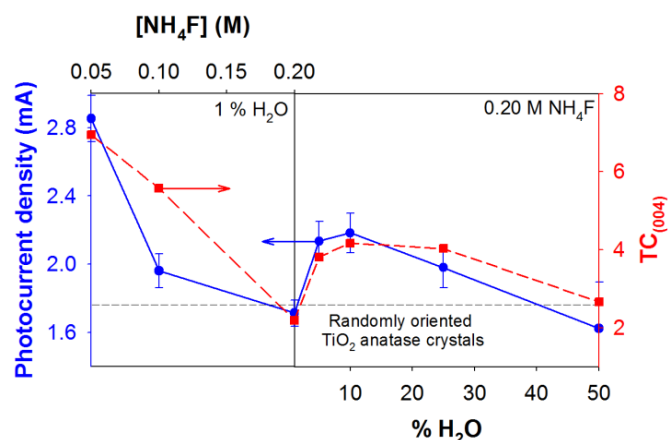


Figure 6. Effect of anodizing bath composition on the measured photocurrent and texture coefficient $TC_{(004)}$ estimated from XRD in Figure 4. Also shown here are the schemes of the crystals and the piling based on the pole diagrams.

It is worth mentioning that XRD is a bulk measurement and the whole sample is being evaluated compared with the SEM or TEM observation that only evaluates a small portion of the sample; in this way, the information obtained from the Rietveld refinement represents a trustable measurement of the orientation degree of anatase crystals.

The obtained results allow us to propose that preferential orientation of anatase crystals in *c*-axis, which gives rise to a fibrous like structure (Figure 3), favors the transport of photogenerated electrons from the outer part of the tube towards the conducting substrate, thus being reflected in an increase in the recorded photocurrent. Therefore, the greatest performance shown by these highly ordered structures is not related to a greater exposure of anatase (001) facets,¹⁶⁻¹⁹ that favors the dissociative adsorption of H₂O,⁴³ but to the improved transport of photogenerated electrons. Further studies are necessary for more thorough understanding of the origin and consequences of preferential orientation of anatase crystals, in order to design more efficient TiO₂ photoanodes.

Conclusions

By varying NH₄F concentration and H₂O content in ethylene glycol based electrolytes, the morphology of the TiO₂ film obtained via anodization was considerably modified causing transition from a nanoporous structure to nanotubes with surface deposits, then nanotubes and finally a sponge like film. Furthermore, anatase crystals formed after heat treatment at 450°C, exhibited a preferential orientation along (004) plane in the films formed in electrolytes containing low NH₄F concentrations (0.05 and 0.10 M), in spite of the possible orientation provided by the oxide film nanotubular structure for the growth of anatase crystals. On the other hand, film composition was also modified depending on the nature of the electrolyte used for its growth due to insertion of F and N from the electrolyte, which had repercussions on optical and semiconducting properties of TiO₂ films.

The photoelectrochemical water oxidation performance of TiO₂ films showed to be dependent on the composition of the electrolyte used to form the porous TiO₂ structure, which may be related to morphological and composition changes. However, the preferential orientation of anatase crystals, quantified by texture coefficient $TC_{(004)}$, was the only variable that showed the same dependence on photoelectrochemical performance as the electrolyte composition. This behavior is associated with anatase crystals piling as fibers along the tube in the [001] direction, normal to the plane of Ti substrate that seems to facilitate the transport of photogenerated electrons towards the conducting substrate.

Acknowledgements

The authors are indebted to the CONACyT for their financial support to carry out this work (Projects CB 2008/105655 and INFR 2011 1 163250). The authors thank to Patricia Castillo, from Laboratorio Central de Microscopía Electrónica (UAM-I) for her assistance in SEM images, Luis Lartundo Rojas, PhD, from Centro de Nanociencias y Micro y Nanotecnologías (UPALM-IPN) for XPS measurements, and to LDRX (T-128) UAM-I for XRD measurements.

Notes and references

^a Universidad Autónoma Metropolitana-Iztapalapa, Av. San Rafael Atlixco 186. Col. Vicentina, 09340, Ciudad de México, D.F. (México).

^b Instituto de Investigaciones en Materiales, Universidad Nacional Autónoma de México, Circuito Exterior S/N, A.P. 70-360, Ciudad de México, D.F. (México).

* corresponding author, e-mail: prosperoacevedopena@yahoo.com

Electronic Supplementary Information (ESI) available: Voltammetric characterization in the dark, XPS spectra, Band-gap measurement from

kubelka-munk approach, semiconducting properties derived from Mott-schottky plots, Rietveld refinement of XRD spectrum and estimation of the corrected $TC_{(004)}$ for nanotube shape. See DOI: 10.1039/b000000x/

- 1 A. Fujishima and K. Honda, *Nature*, 1972, **238**, 37-38.
- 2 A.L. Linsebigler, G. Lu and J.T. Yates, *Chem. Rev.*, 1995, **95**, 735-758.
- 3 J.T. Carneiro, A.R. Almeida, J.A. Moulijn and G. Mul, *Phys. Chem. Chem. Phys.*, 2010, **12**, 2744-2750.
- 4 M.A. Henderson, *Surf. Sci. Rep.*, 2011, **66**, 185-297.
- 5 G. Waldner and J. Krýsa, *Electrochim. Acta.*, 2005, **50**, 4498-4504.
- 6 M. Radecka, A. Trenczek-Zajac, K. Zakrzewska and M. Rekas, *J. Power Sources*, 2007, **173**, 816-821.
- 7 P. Acevedo-Peña, G. Vázquez, D. Laverde, J. E. Pedraza-Rosas, J. Maríquez, and I. González, *J. Electrochem. Soc.*, 2009, **156**, C377-C386.
- 8 F. Zhu, H. Dong, Y. Wang, D. Wu, J. Li, J. Pan, Q. Li, J. Zhang and D. Xu, *Phys. Chem. Chem. Phys.*, 2013, **15**, 17798-17803.
- 9 L. Căi, I.S. Cho, M. Logar, A. Mehta, J. He, C.H. Lee, P.M. Rao, Y. Feng, J. Wilcox, F.B. Prinz and X. Zheng, *Phys. Chem. Chem. Phys.*, 2014, **16**, 12299-12306.
- 10 P. Roy, S. Berger and P. Schmuki, *Angew. Chem. Int. Ed.*, 2011, **50**, 2904-2939.
- 11 Paramasivam, H. Jha, N. Liu and Schmuki, P. *Small*, 2012, **8**, 3073-3103.
- 12 B. Chen, J. Hou and K. Lu, *Langmuir*, 2013, **29**, 5911-5919.
- 13 S. Liang, J. He, Z. Sun, Q. Liu, Y. Jiang, H. Cheng, B. He, Z. Xie and S. Wei, *J. Phys. Chem. C*, 2012, **116**, 9049-9053.
- 14 P. Acevedo-Peña and I. González, *J. Electrochem. Soc.*, 2013, **160**, H452-H458.
- 15 L-K. Tsui, T. Homma and G. Zangari, *J. Phys. Chem. C*, 2013, **117**, 6979-6989.
- 16 M-H. Jung, M-J. Chu and M.G. Kang, *Chem. Commun.*, 2012, **48**, 5016-5018.
- 17 S. Lee, I.J. Park, D.H. Kim, W.M. Seong, D.W. Kim, G.S. Han, J.Y. Kim, H.S. Jung and K.S. Hong, *Energy Environ. Sci.*, 2012, **5**, 7989-7995.
- 18 Z. Yang, Z. Ma, D. Pan, D. Chen, F. Xu and S. Chen, *Ceram. Int.*, 2014, **40**, 173-180.
- 19 P. Acevedo-Peña, J.E. Carrera-Crespo, F. González and I. González, *Electrochim. Acta*, 2014, **140**, 564-571.
- 20 P. Acevedo-Peña, L. Lartundo-Rojas and I. González, *J. Solid State Electrochem.*, 2013, **17**, 2939-2947.
- 21 A.F. Carley, P.R. Chalker, J.C. Riviere and M.W. Roberts, *J. Chem. Soc. Faraday Trans. 1*, 1987, **83**, 351-370.
- 22 B. Siemsmeyer and J.W. Schultze, *Surf. Interface Anal.*, 1990, **16**, 309-314.
- 23 R.L. Kurtz and V.E. Henrich, *Surf. Sci. Spectra*, 1998, **5**, 179-181.
- 24 Z. Xia, H. Nanjo, T. Aizawa, M. Kanakubo, M. Fujimura and J. Onagawa, *Surf. Sci.*, 2007, **601**, 5133-5141.
- 25 Milošev, T. Kosec and H-H. Strehlow, *Electrochim. Acta*, 2008, **53**, 3547-3558.
- 26 P. Acevedo-Peña, J. Vázquez-Arenas, R. Cabrera-Sierra, L. Lartundo-Rojas and I. González, *J. Electrochem. Soc.*, 2013, **160**, C277-C284.

- 27 W. Dabrowski, P. Grybos, P. Hottowy, K. Swientek and P. Wiacek, *Nucl. Instrum. Methods Phys. Res. Sect. A*, 2003, **512**, 213-219.
- 28 R.W. Cheary and A.A. Coelho, *J. Appl. Cryst.*, 1992, **25**, 109-121.
- 29 TOPAS V4.2: *General profile and structure analysis software for powder diffraction data. User's manual*, Bruker AXS, Karlsruhe, Germany, **2009**.
- 30 G. Höelzer, M. Fritsch, M. Deutsch, J. Härwig and E. Föster, *Phys. Rev. A*, 1997, **56**, 4554-4568.
- 31 M.J. Järvinen, *J. Appl. Crystallogr.*, 1993, **26**, 525-531.
- 32 P. Frey, *MEDIT: An interactive mesh visualization software, Technical Report RT-0253*, Institut National de Recherche en Informatique et en Automatique, **2001**.
- 33 X. Bokhimi and R. Zanella, *J. Phys. Chem. C*, 2008, **112**, 12463-12467.
- 34 S. Yoriya and C.A. Grimes, *J. Mater. Chem.*, 2011, **21**, 102-108.
- 35 S. Yoriya, N. Bao and C.A. Grimes, *J. Mater. Chem.*, 2011, **21**, 13909-13912.
- 36 A.G. Kontos, A.I. Kontos, D.S. Tsoukleris, V. Likodimos, J. Kunze, P. Schmuki and P. Falaras, *Nanotech.*, 2009, **20**, 045603.
- 37 K. Shankar, J.I. Basham, N.K. Allam, O.K. Varghese, G.K. Mor, X. Feng, M. Paulose, J.A. Seabold, K.-S. Choi and C.A. Grimes, *J. Phys. Chem. C*, 2009, **113**, 6327-6359.
- 38 M. Jankulovska, I. Barceló, T. Lana-Villarreal and R. Gómez, *J. Phys. Chem. C*, 2013, **117**, 4024-4031.
- 39 M.V. Dozzi and E. Selli, *J. Photochem. Photobiol. C*, 2013, **14**, 13-28.
- 40 D. Ariosa, F. Elhordoy, E.A. Dalchiele, R.E. Marotti and C. Stari, *J. Appl. Phys.*, 2011, **110**, 124901.
- 41 C. Barret and T.B. Massalski, *Structure of Metals*, Pergamon, Oxford, 1980, pp 1923-1924.
- 42 D. Kim, A. Ghicov and P. Schmuki, *Electrochem. Commun.*, 2008, **10**, 1835-1838.
- 43 M. Sumita, C. Hu and Y. Tateyama, *J. Phys. Chem. C*, 2010, **114**, 18529-18537.